CHEMISTRY
A EUROPEAN JOURNAL

DOI: 10.1002/chem.201001264

Nanoscale Self-Hosting of Molecular Spin-States in the Intermediate Phase of a Spin-Crossover Material

Nicolas Bréfuel,[a, b, f] Eric Collet,*[c] Hiroshi Watanabe,[d] Masaaki Kojima,[e] Naohide Matsumoto,[b] Loic Toupet,[c] Koichiro Tanaka,[d] and Jean-Pierre Tuchagues*[a]

Dedicated to the memory of Professor Hans Toftlund

Abstract: A new spin-crossover (SC) complex $[Fe^{II}H_2L^{2\text{-}Me}][AsF_6]_2$ has been synthesized, in which $H_2L^{2\text{-}Me}$ denotes the chirogenic hexadentate N_6 Schiff-base ligand bis{[(2-methylimidazol-4-yl)methylidene]-3-aminopropyl}ethylenediamine. This complex has revealed a rich variety of phases during its two-step thermal crossover, as well as photoinduced spin-state switching. A high-symmetry high-spin (HS, S = 2) phase, a low-symmetry low-spin (LS, S = 0) phase, an intermediate phase characterized by an unprecedented lozenge pattern of 12 predominantly HS molecular crystallographic sites confining 18 predominantly LS molecular crystallographic sites, and a photoinduced low-symmetry HS phase have been accurately evidenced by temperature-dependent magnetic susceptibility, Mössbauer spectroscopy, and crystallographic studies. This variety of phases illustrates the multi-stability of this system, which results from coupling between the electronic states and structural instabilities.

Keywords: ferrous materials · magnetic properties · Moessbauer spectroscopy · photomagnetic studies · spin crossover

Introduction

Confinement of molecules opens up new possibilities for studying matter on the nanometer scale. Well-known examples are interacting host–guest systems that may enter into various types of inclusion compounds.[1] One of the main challenges is not only to isolate molecules in a given state, but also to tune them between different states at such ultimate scales. Among multistable molecular systems,[2] spin-crossover (SC) compounds are prototype switchable materials, for which the constituent molecules based on $3d^4$–$3d^7$ transition-metal complexes may be switched between high-spin (HS) and low-spin (LS) states.[3a] They have been the subject of intense investigation over the last decades because of possible applications as molecular switches and electronic data storage devices.[3b] The race toward nanoscale switchable devices has led to nanoscale SC molecular assemblies, crystals, films, and particles through top-down or bottom-up approaches.[4–8]

The cubic crystal field determines the energy minima for the LS and HS potential surfaces of d^4–d^7 ions in octahedral ligand environments. An entropy-driven SC may be observed when the energy gap between the LS and HS potential minima is comparable to k*T*. However, the crystal field depends not only on the direct ligand environment, but also

[a] Dr. N. Bréfuel, Prof. J.-P. Tuchagues
LCC (Laboratoire de Chimie de Coordination) UPR-CNRS 8241
205, route de Narbonne, 31077 Toulouse and Université
de Toulouse; UPS, INPT; LCC; 31077 Toulouse (France)
Fax: (+33) 561-553003
E-mail: jean-pierre.tuchagues@lcc-toulouse.fr

[b] Dr. N. Bréfuel, Prof. N. Matsumoto
Department of Chemistry, Faculty of Science, Kumamoto University
Kurokami 2-39-1, Kumamoto 860-8555 (Japan)

[c] Prof. E. Collet, Dr. L. Toupet
Institut de Physique de Rennes, UMR CNRS 6251
Université Rennes 1, 263 avenue Général Leclerc
35042 Rennes cedex (France)
Fax: (+33)223-236717
E-mail: eric.collet@univ-rennes1.fr

[d] Dr. H. Watanabe, Prof. K. Tanaka
Institute for Integrated Cell-Material Sciences, Kyoto University
Sakyo-ku, Kyoto 606-8501 (Japan), and CREST (Japan)
Science and Technology Agency, Kawaguchi
Saitama 332-0012 (Japan)

[e] Prof. M. Kojima
Department of Chemistry, Faculty of Science, Okayama University
Tsushima-naka 3-1-1, Okayama 700-8530 (Japan)

[f] Dr. N. Bréfuel
Present address: Laboratoire National des Champs
Magnétiques Intenses, UPR 3228, 25, avenue des Martyrs
38042 Grenoble cedex 9 (France)

on the more distant environment. The volume change of the first coordination sphere of each metal center upon LS to HS SC is sensed by the surrounding molecules through the crystal lattice.[9] Two strategies have been developed to promote communication between neighboring molecules: the polymeric approach is based on covalent linkages between metal centers, whereas the supramolecular approach uses weaker interactions such as H-bonding, π–π stacking, and/or van der Waals interactions. Many supramolecular assemblies[10] and polymeric[11] compounds have already been investigated, displaying remarkable cooperative phenomena, such as first-order transition with a hysteresis loop[12a] or two-step crossover,[12b,c] for which ordering of electronic states may take place at the nanometer scale. However, the microscopic origin of cooperativity has not yet been fully identified and in-depth studies of the structural and chemical factors controlling the characteristics of SC are necessary to get a better understanding of the mechanism(s) involved, and to design new systems that may be used in molecular electronics.[3b,12a,13] In addition, the ordering of electronic states and the concomitant symmetry breaking may both result from coupling between different types of electronic and structural instabilities. This concept, although general in material science,[14] has not yet been widely discussed in relation to SC materials.[15]

Few examples of mononuclear molecular materials undergoing a two-step SC associated with an intermolecular reorganization in the broken symmetry phase, the so-called intermediate (INT) phase, involving a fractional population of the HS state, have been reported.[16,17] In a very few cases, the INT phase has been fully described by diffraction techniques, evidencing HS-LS,[12b,18] LS-HS-LS,[19] or LS-HS-HS-LS[20] long-range or short-range ordering.[16] With one exception (a one-dimensional chain polymeric material[16]), the "communication network" between SC units is mediated by H-bond networks in all examples. However, two different types of "communication network" may be distinguished among the latter materials: either SC molecules are directly H-bonded through ligand(s),[10f,g,12b,19] or out-of-sphere counter anions link SC complex cations through dense H-bond networks.[17,18a,b,20] Interconnecting two types of chemical species, such as a neutral polydentate ligand of the complex cation (yielding the appropriate ligand field range at the SC center: intramolecular function) to out-of-sphere anions (allowing a fine-tuning of the ligand field and participating in intermolecular interactions with the former), is a more flexible approach for controlling both the communication network and crystal lattice properties, the latter importantly through the shape and size of the out-of-sphere counteranion. This is the approach we propose for further exploring the remarkable cooperative phenomena associated with structural versatility.

In this contribution, we report the unusual SC behavior of a new complex, $[Fe^{II}H_2L^{2\text{-}Me}][AsF_6]_2$ (**1**), associated to the confinement of LS molecular crystallographic sites in a nanometer cage defined by HS molecular crystallographic sites ($H_2L^{2\text{-}Me}$ denotes the chirogenic hexadentate N_6 Schiff-base ligand bis{[(2-methylimidazol-4-yl)methylidene]-3-aminopropyl}ethylenediamine). The synthesis and temperature-dependent magnetic, Mössbauer, and X-ray diffraction measurements of **1** are described and interpreted. Special emphasis is devoted to the symmetry breakings observed in the low-temperature LS and photoinduced HS phases, and to the unique long-range ordering of the INT phase based on an unprecedented lozenge pattern including 12 predominantly HS, 8 predominantly LS, and 10 purely LS molecular crystallographic sites.

Results and Discussion

Synthesis and characterization: Complex **1** was prepared through anaerobic reaction of freshly synthesized $H_2L^{2\text{-}Me}$ Schiff-base ligand[21] with $Fe^{II}Cl_2{\cdot}4H_2O$ in ethanol, followed by anion metathesis[20] with $NaAsF_6$. In this way, **1** was anaerobically obtained exclusively as orange single crystals, which were deposited from the filtered reaction medium. The chemical composition and purity of $[Fe^{II}H_2L^{2\text{-}Me}][AsF_6]_2$ (**1**) were established through elemental analysis and IR spectroscopy, while the crystal structure confirmed the molecular organization into $[Fe^{II}H_2L^{2\text{-}Me}]^{2+}$ complex cations associated with $[AsF_6]^-$ complex anions in a 1:2 ratio through a dense three-dimensional network of H-bonds. An ORTEP drawing of the $[Fe^{II}H_2L^{2\text{-}Me}]^{2+}$ complex cation of **1** is shown in Figure 1.

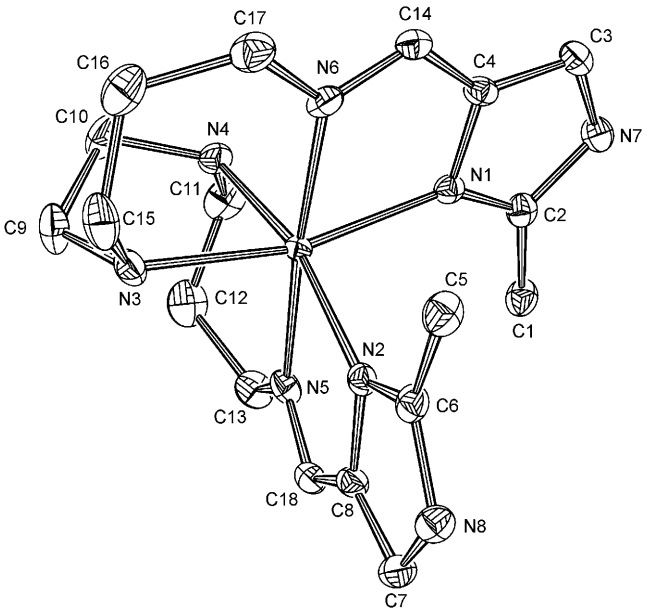

Figure 1. ORTEP drawing of the $[FeH_2L^{2\text{-}Me}]^{2+}$ complex cation of **1** at 250 K with the atom-numbering scheme. H atoms are omitted for clarity, and thermal ellipsoids are drawn at the 50% probability level.

Magnetic properties: The magnetic behavior of **1** was studied by magnetic susceptibility measurements. The gradual thermal variation of the $\chi_M T$ product of **1** was indicative of

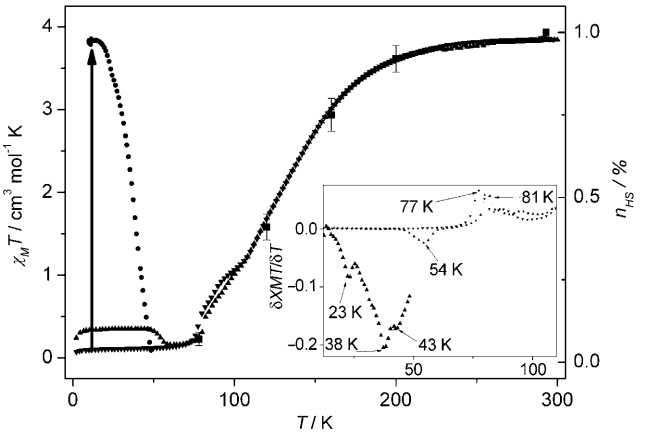

Figure 2. Temperature dependence of $\chi_M T$ in the 2–300 K range for **1**. The sample was first quickly cooled from 300 to 2 K and the susceptibility was subsequently measured upon warming (▲) and then cooling the sample (▼) at a sweep rate of 2 K min^{-1}; (●) shows the temperature dependence of $\chi_M T$ at the same sweep rate, after irradiating the sample at 10 K with a 532 nm laser. (■) Error bars represent the n_{HS} fraction obtained from selected ^{57}Fe Mössbauer spectra. Inset: Plot of $d\chi_M T/dT$ versus temperature, indicating T(LIESST) (23, 38 K), T(TIESST) (54 K), $T\uparrow$ (81 K), and $T\downarrow$ (77 K) values at the minima.

a complete two-step SC (Figure 2). Upon lowering the temperature, $\chi_M T$ decreased from a value at 300 K typical of an HS ($S=2$) state (≈ 3.8 cm^3 mol^{-1} K) to a value at 2 K typical of an LS ($S=0$) state (≈ 0.1 cm^3 mol^{-1} K).

Two different steps were observed: a large decrease between 240 and 110 K and a smaller one between about 90 and 74 K. A pseudo plateau centered at about 100 K, at which the HS molecular fraction n_{HS} reached about 29% ($\chi_M T = 1.1$ cm^3 mol^{-1} K), was observed between the two steps. Upon increasing the temperature from 2 K (following a fast cooling), a small difference compared with the measurement upon slow cooling was observed at low temperature: a larger $\chi_M T$ value (≈ 0.4 cm^3 mol^{-1} K, that is, ≈ 10% of HS state) was measured, which remained essentially constant up to 48 K, indicating a small frozen-in effect. The T-(TIESST) value (TIESST = thermally induced excited spin-state trapping), defined as the minimum of the $d\chi_M T/dt$ versus T curve, was measured as 54(1) K. It is important to note that the presence of two different steps in both the heating and cooling modes, and the narrow hysteresis associated with the smaller and steeper low-temperature step, have been reproducibly observed for several samples of **1** derived from different syntheses. Because materials showing TIESST usually show light-induced excited spin-state trapping (LIESST),[22] we investigated the magnetic behavior of **1** upon irradiation at 10 K with continuous-wave laser light (1 mW mm^{-2}) of $\lambda = 532$ nm, which has been demonstrated to be an efficient wavelength for switching this Fe^{II} cation from LS to HS.[20] Complex **1** was found to exhibit a quantitative light-induced effect (LIESST):[23] within 1 h, the $\chi_M T$ product increased from an initial value of about 0.1 cm^3 mol^{-1} K to a saturation regime at 3.8 cm^3 mol^{-1} K, evidencing quantitative photo-commutation. Once the irradiation was stopped, the relaxation upon increasing T (1 K min^{-1}) occurred in two steps, a small one at 23 K (ca. 12% of Fe^{II} sites) and a large one centered at around 38 K (minima of the $d\chi_M T/dt$ versus T curve), suggesting complex relaxation dynamics. The tiny discontinuity at 43 K is regarded as an artefact.

Mössbauer spectroscopy: The HS fraction at different temperatures, plotted in Figure 2 (black diamonds), together with $\chi_M T$, was deduced from Mössbauer measurements[24] on **1**. The fitted Mössbauer spectra and the corresponding parameters are reported in Figure 3 and Table 1, respectively.

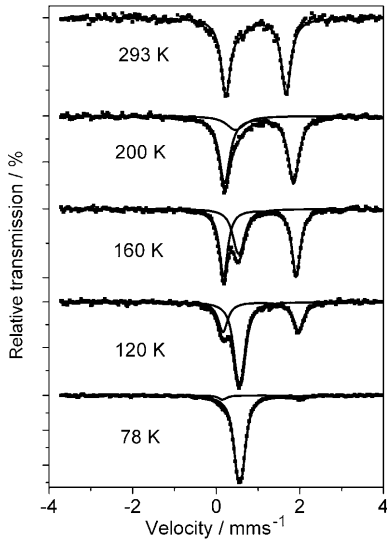

Figure 3. Selected Mössbauer spectra of **1**: solid lines correspond to HS and LS sites.

Table 1. Mössbauer data for **1**. Isomer shifts (δ, mm s^{-1}) refer to metallic iron at room temperature; quadrupole splittings (ΔE_Q, mm s^{-1}); Γ = half-width of the lines (mm s^{-1}); statistical standard deviations are given in parentheses; underlined values were fixed for the fit.

T/K	δ (LS)	ΔE_Q (LS)	Γ (LS)	δ (HS)	ΔE_Q (HS)	Γ (HS)	% HS
78	0.561(2)	0.112(5)	0.122(4)	1.09(2)	1.87(4)	0.12(3)	7(2)
120	0.556(4)	0.11(2)	0.126(9)	1.065(7)	1.81(2)	0.14(1)	41(4)
160	0.540(8)	0.10(5)	0.14(2)	1.045(3)	1.735(6)	0.121(5)	71(5)
200	0.47(3)	0.09	0.25	1.025(4)	1.649(7)	0.155(5)	90(4)
293	–	–	–	0.955(5)	1.433(9)	0.146(7)	100

A good agreement between Mössbauer and magnetic measurements was observed over the whole temperature range: the HS fraction reaches about 0.29 on the plateau, whereas it equals 1 above 240 K and 0 below 60 K.

Structure of the 250 K HS phase: Crystal structures of **1** were determined by single-crystal X-ray diffraction analysis at 250 K (HS), 100 K (INT, ca. 25% HS/75% LS), 15 K (LS), and in the photoinduced HS state (PIHS) at 15 K (Table 2). At each temperature, the Fe^{II} ion assumes a dis-

Table 2. Crystallographic data for **1** at 250 (HS), 100 (INT), and 15 K (LS, PIHS).

Crystal phase	HS	INT	LS	PIHS
T [K]	250	100	15	15 (532 nm)
formula	$FeC_{18}H_{30}N_8As_2F_{12}$			
Fw [g mol^{-1}]	792.1608			
crystal system	orthorhombic			
space group	$P22_12_1$	$P22_12_1$	$P2_12_12_1$	$P22_12_1$
a [Å]	8.4897(10)	8.2451(7)	32.746(3)	8.2713(2)
b [Å]	9.505(2)	47.197(4)	9.4540(10)	9.2634(4)
c [Å]	17.543(2)	52.289(4)	17.2850(10)	53.051(3)
V [Å^3]	1415.6(4)	20348(3)	5351.1(8)	4064.8(3)
cation/unit cell	2	30	8	6
F(000)	788	11820	3152	2364
ρ_{calcd} [Mg m^{-3}]	1.939	1.94	1.967	1.942
$\mu(Mo_{K\alpha})$ [mm^{-1}]	2.957	3.086	3.129	3.090
θ [° min–max]	2.7–27	2.6–27	2.5–27	2.5–27
collected data	19077	327568	89971	15766
unique data	3099	39715	11221	4620
R(int)	0.02	0.087	0.0384	0.119
var. param.	187	1345	739	270
obsd. refl.	2853	12362	8269	8740
R obsd., all	0.027	0.14	0.0389	0.15
R_w obsd., all	0.030	0.26	0.0634	0.30

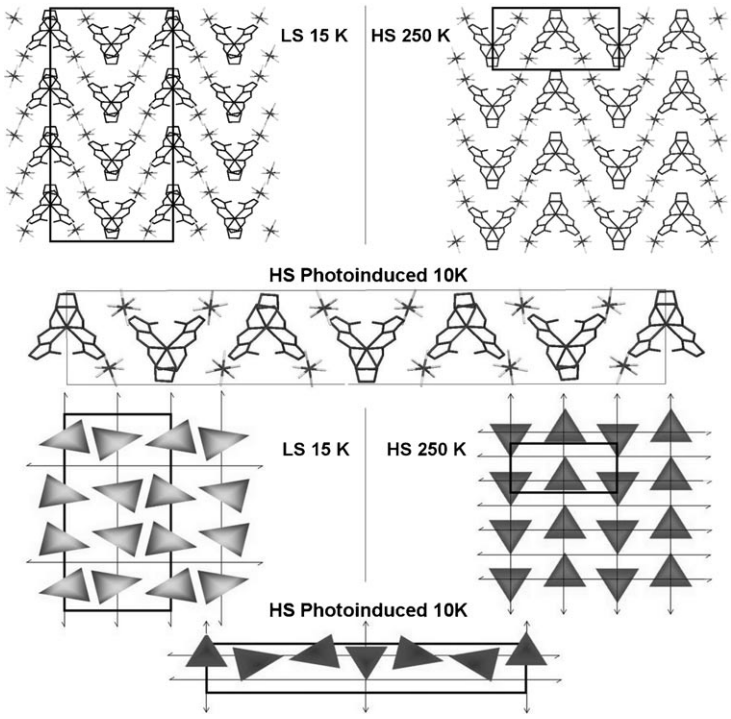

Figure 4. Top: Crystal structure of **1** in the (*a*,*c*) plane (*a* vertical): LS phase (top left, 15 K with a *4a*, *b*, *c* cell), HS phase (top right, 250 K with an *a*, *b*, *c* cell), and photoinduced HS state (bottom with an *a*, *b*, *3c* cell). Bottom: Corresponding schematic representation of the cations, viewed as triangles along the *b* axis, and symmetry operators. Unit cells are schematized by rectangles.

torted octahedral coordination environment involving the six N donor atoms of the chirogenic hexadentate Schiff base: two Fe–N(imine), two Fe–N(amine), and two Fe–N(imidazolyl) bonds (Figure 1). Complex **1** assumes a three-dimensional (3D) supramolecular structure in which $[AsF_6]^-$ anions connect neighboring $[Fe^{II}H_2L^{2\text{-}Me}]^{2+}$ cations through N–H···F hydrogen bonds, yielding layers of metal cations separated by layers of counteranions in all of the structures (Figure 4). In the $P22_12_1$ unit cell at 250 K, all metal centers are symmetry-equivalent and have an average Fe–N bond length of 2.187(3) Å (Table 3), typical of Fe^{II} complexes in the HS state. The $[Fe^{II}H_2L^{2\text{-}Me}]^{2+}$ complex cations are located on the two-fold axis (Figure 4) and the $[AsF_6]^-$ complex anions are in general positions, yielding an asymmetric unit consisting of half a cation and one anion.

Table 3. Coordination bond lengths [Å] for **1** in the HS, LS, and PIHS phases.

Fe–N	HS 250 K	Fe1 LS 15 K	Fe2	Fe1 PIHS 15 K	Fe2
Fe–N1	2.174(2)	2.025(4)	2.031(4)	2.18(2)	2.17(2)
Fe–N2	2.189(2)	2.030(4)	2.025(4)	2.14(2)	2.08(2)
Fe–N3	2.198(3)	2.039(4)	2.035(4)	2.16(2)	2.21(2)
Fe–N4	2.174(2)	2.031(4)	2.036(4)	2.22(2)	2.17(2)
Fe–N5	2.189(2)	2.014(4)	2.014(4)	2.22(2)	2.08(2)
Fe–N6	2.198(3)	2.013(4)	2.010 (4)	2.25(2)	2.21(2)
Fe–N[a]	2.187	2.023		2.17	

[a] Average bond lengths.

Modulated structure of the LS phase at 15 K: At 15 K, complex **1** is in the LS state and a symmetry breaking occurs: the unit cell changes from *a*, *b*, *c* (HS 250 K) to 4*a*, *b*, *c* (quadruplicate *a* axis, LS 15 K) with a change of space group to $P2_12_12_1$, yielding two non-equivalent LS ions (8 per unit cell). The combination of the translational symmetry 2*a* in the HS phase and two-fold axis corresponds to the 2_1 screw axis in the LS phase (4*a*, *b*, *c*). As a result of the loss of the two-fold axis, the symmetry breaking is associated with tilting, deformation, and displacement of the different ions. Note that the cations, which are no longer located on the two-fold symmetry axis, have moved from the Wyckoff position, as schematically depicted in Figure 4. Therefore, the asymmetric unit consists of two cations and four anions. The displacement of the cations from the two-fold axis can be estimated from the coordinates of the Fe1 and Fe2 atoms. The corresponding relative displacements of Fe1 and Fe2 are about 0.3 Å along *a*, 0.17 Å along *b*, and 0.15 Å along *c*. Similar displacements are observed for the AsF_6 anions. Therefore, the LS phase can be discussed in terms of a modulated structure; both types of modulation (displacement and rotation) can be observed in Figure 5. The average Fe–N bond length for both sites (Fe1–N = 2.025(4) and Fe2–N = 2.021(4) Å; Table 3) is typical of LS Fe^{II} with six N donors.

Broken symmetry structure of the PIHS phase: Structural analysis of the photoinduced transitions gives key insight into the molecular reorganization that stabilizes the photoinduced state.[25] The photoinduced HS state was generated from the LS phase by laser excitation at 532 nm. The structural analysis indicated that the unit cell changed to *a*, *b*, 3*c*

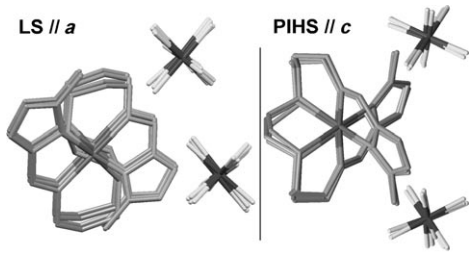

Figure 5. Projections of the structure of the LS phase at 15 K along the multiplied *a* axis (left) and projections of the structure of the PIHS phase at 15 K along the multiplied *c* axis (right), showing the motions of the ions in the structure of $[Fe^{II}H_2L^{2\text{-}Me}][AsF_6]_2$.

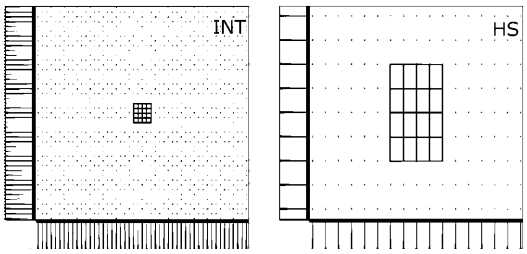

Figure 6. Projection of the Bragg peaks along *a** in the reciprocal space in the high-symmetry HS phase (right, 120 K) and in the INT phase (left, 100 K) for **1**. The periodicity is changed by a factor 5 along *b** (vertical) and by a factor 3 along *c** (horizontal).

(triplicate *c* axis, PIHS 15 K). The $P22_12_1$ space group of the PIHS phase is an isomorphic sub-group of lower index of the HS phase at 250 K. There are two independent HS cations per unit cell (Figure 4) with comparable average Fe–N bond lengths for both Fe^{II} centers (Fe–N ≈ 2.17(2) Å), typical of HS Fe^{II} (Table 3). This is similar to what was observed for $[Fe^{II}H_2L^{2\text{-}Me}][PF_6]_2$ (**2**),[20] and the symmetry breaking with respect to the HS phase at 250 K is also associated with molecular distortion/rotation/displacements of the layers, which are no longer located on the two-fold symmetry axis (Figure 4). Although the asymmetric unit consists of one entire plus one half-cation and three anions, only the entire cation (Fe2) remains located on the two-fold axis. Fe1 moves with respect to Fe2 by about 0.1 Å along *a*, 0.08 Å along *b*, and 0.15 Å along *c*. Such structural instability has also been reported for other compounds, for which the modulated location of metastable HS molecules at low temperature yielded a triplicate cell parameter.[26]

Spin-state ordering of the INT phase: The most unusual behavior of the present compound is the appearance of a complex structure in the intermediate phase corresponding to the partial SC at the approximately 100 K centered plateau. This new phase results from a symmetry breaking among crystallographically equivalent cation sites. This ordering differs significantly from any type of INT phase hitherto reported for SC compounds, which have resulted from regular alternation of HS and LS states along a given crystal axis for short-range[16] or long-range HS-LS,[12b,17,18] LS-HS-LS,[19] or LS-HS-HS-LS[20] ordering. In the INT phase of **1**, a more complex change is observed toward an unprecedented *a*, 5*b*, 3*c* cell. The simultaneous quintuplicate *b* and triplicate *c* axes are characterized by the appearance of numerous Bragg peaks in the reciprocal space (novel translational symmetry; Figure 6). The temperature dependence of the intensities of the Bragg peaks characterizing this INT phase is shown in Figure 7. Upon decreasing the temperature, the peaks characterizing the (*a*, 5*b*, 3*c*) INT phase discontinuously appeared at around 110 K and disappeared at around 85 K, whereupon the Bragg peaks associated with the quadruplicate cell along *a* characterizing the (4*a*, *b*, *c*) LS phase started to appear.

Both phases (and the corresponding Bragg peaks) coexist in the vicinity of the hysteresis observed by magnetic measurements at around 85 K. It should be noted that small discontinuities in the crystal volume were observed around both phase transition temperatures (in the INT phase, the unit cell volume is 15 times larger). The discontinuous changes in the intensity of the Bragg reflections and volume, as well as the coexistence of phases, point to the first-order nature of both transitions (at around 110 and 85 K).

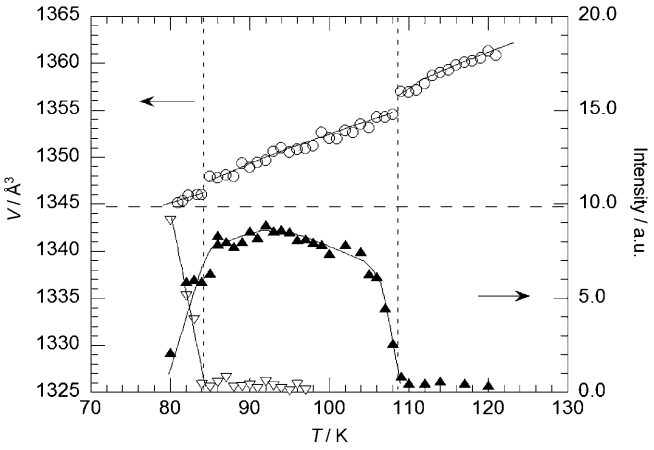

Figure 7. Temperature dependence of the unit-cell volume (given in the *a*, *b*, *c* cell, HS state) and of the intensity of the Bragg peaks related to the different symmetry breakings that occur in the INT and LS phases; ▲ = *a*, 5*b*, 3*c*; ▽ = 4*a*, *b*, *c*; ○ = V.

We have been able to solve and refine the structure of the INT phase in the (*a*, 5*b*, 3*c*) $P22_12_1$ cell. However, because of the pseudosymmetry, important correlations were observed during the refinement. Compared with the structure of the HS state (250 K), the number of parameters to refine is multiplied by 15 (5 × 3). However, because of the low intensity of the peaks related to the new cell, the number of observed Bragg reflections (11588) is not 15 times larger than that for the HS phase (2853) but only about four times larger (many new peaks are too weak to be measured). Therefore, we refined the structure with isotropic thermal motion factors to reduce the number of parameters. In the structure of this INT phase, the symmetry breaking results from simultaneous loss of the translational symmetry along *b* and *c*. Because of the limited remaining number of *2*- and 2_1-fold axes, there are eight independent cations (Fe sites

are labeled Fe1–Fe8) among the 30 cations of the INT phase cell and only one of them (Fe8) remains on a two-fold axis. Figure 8 shows the spatial distribution of the eight independent sites within the unit cell. Inspection of the Fe–N bond lengths reported in Table 4 for the different independent cations in the cell provides an interesting insight into the spatial distribution of HS and LS states among the 30 sites constituting the supercell (Figure 8). Twelve complex cation sites(red) (three independent sites Fe2, Fe5, Fe6) with longer bond lengths (Fe–N ≈ 2.12–2.15 Å) are mainly in the HS state. Ten cation sites (blue) with shorter bond lengths (Fe–N ≈ 1.95–2.01 Å; independent sites Fe1, Fe4, Fe8) are in the LS state. Finally, eight cation sites (purple) (independent sites Fe3, Fe7) have intermediate bond lengths (Fe–N = 2.04, 2.06 Å).

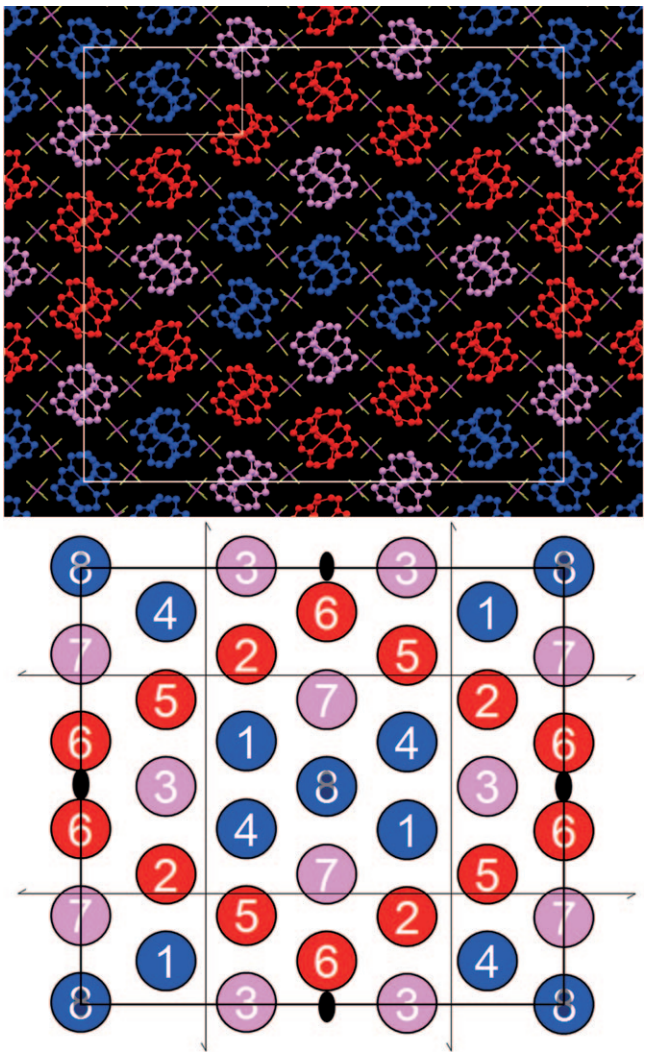

Figure 8. Crystal packing of the INT phase in the (*b*,*c*) plane at 100 K. The large box is the (*a* 5*b* 3*c*) cell and the small one is the (*a b c*) unit cell of the HS phase. Red, purple, and blue sites correspond to HS fractions equal to 0.75, 0.2, and 0%, respectively. A schematic drawing of the different independent sites with labeling is shown below.

Table 4. Coordination bond lengths [Å] for **1** in the INT phase at 100 K.

	Fe–N1	Fe–N2	Fe–N3	Fe–N4	Fe–N5	Fe–N6	Fe–N[a]
Fe1	2.00(1)	2.03(1)	2.05(2)	2.00(1)	1.94(1)	2.02(1)	2.00
Fe2	2.09(2)	2.19(1)	2.14(2)	2.13(1)	2.10(1)	2.13(2)	2.13
Fe3	2.00(1)	2.02(2)	2.03(2)	2.05(1)	2.05(1)	2.09(1)	2.04
Fe4	2.06(1)	2.00(1)	2.05(2)	2.04(2)	1.98(1)	1.95(1)	2.01
Fe5	2.17(1)	2.09(1)	2.12(2)	2.11(1)	2.09(1)	2.15(2)	2.12
Fe6	2.14(2)	2.16(1)	2.15(1)	2.17(2)	2.17(2)	2.12(2)	2.15
Fe7	2.04(1)	2.02(1)	2.07(2)	2.08(1)	2.07(1)	2.12(2)	2.06
Fe8	1.95(1)	1.95(1)	1.92(1)	1.92(1)	1.97(1)	1.97(1)	1.95

[a] Average bond length.

The resulting spin-state ordering pattern is based on a sub-lattice of HS molecules describing a lozenge pattern. Here again, the symmetry breaking involves displacement and rotation of the ions (Figure 9). Note that this incomplete ordering phenomenon induces different HS populations over the different molecular sites. In other words, the present phase transition generates a crystal structure in which molecules are confined in an electronic LS state at the nanometer scale, surrounded by molecules in the HS state. The internal dimensions of the lozenge-section channel are 4.5 × 3.2 nm.

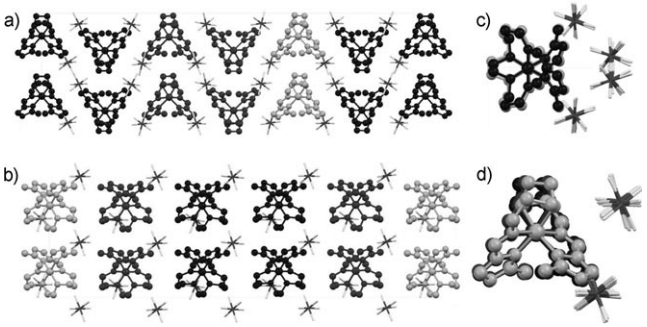

Figure 9. Slices in the (*a*,*c*) plane (a) and in the (*a*,*b*) plane (b) of the INT phase structure of **1**. Projections along the *c* (c) and *b* (d) axes showing ion displacements and reorientations.

By assuming, in a first approximation, a linear variation of Fe–N with the HS fraction, one can estimate the HS fraction: at red sites $n_{HSr} \approx 0.75$, at purple sites $n_{HSp} \approx 0.2$, and at blue sites $n_{HSb} \approx 0$ (Figure 8). The resulting rough estimate of the average n_{HS} fraction over the unit cell $\{(12 \times 0.75 + 8 \times 0.2 + 10 \times 0)/30 = 0.35(8)\}$ is in quite good agreement with the value obtained for the plateau through magnetic measurements. As can be observed in Figure 9, the symmetry breaking is also associated with intermolecular reorganization, resulting in a spatial modulation of the reorientation and position of the anions and cations. From a physical viewpoint, this ordering phenomenon of molecular spin-states in an INT phase is very different from the case of compounds with crystallographically independent sites, which may display different thermal behavior and different HS populations without symmetry breaking.[26,27]

Phase diagram and symmetry-breaking order parameters: When the cell translational symmetry changes to (*a*, 5*b*, 3*c*), at least two symmetry-breaking order parameters (OP),

which do not transform according to the same irreducible representation, have to be involved. For example, one (η) may be associated with the cell triplication along *c* and the other (ξ) with the cell quintuplication along *b*. The theory of phase transitions described by two order parameters has been reported in the literature.[28] The non-equilibrium potential is developed as a power law of the two order parameters according to Equation (1):

$$\Phi = a_1\eta^2 + a_2\eta^4 + a_3\eta^6 + b_1\xi^2 + b_2\xi^4 + b_3\xi^6 + \gamma\eta^2\xi^2 \qquad (1)$$

in which a_i, b_i, and γ are phenomenological parameters. a_1 and b_1 depend linearly on the temperature and pressure.

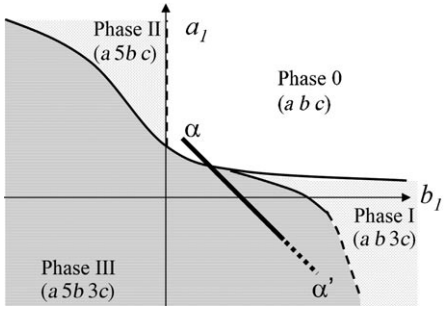

Figure 10. Phase diagram of two coupled order parameters (modified from ref. [28]). First-order transitions are indicated by continuous lines and second-order transitions by discontinuous lines.

In such a case, four phases are possible, as sketched in Figure 10: phase 0 (the high-symmetry phase for which $\eta = \xi = 0$) and three low-symmetry phases, phase I ($\eta \neq 0$, $\xi = 0$), phase II ($\eta = 0$, $\xi \neq 0$), and phase III ($\eta \neq 0$, $\xi \neq 0$). In the present case, phase 0 is the HS high-symmetry state. Phase I, in which only one type of symmetry breaking occurs, is the PIHS state (the OP associated with the change to 3*c* is $\eta \neq 0$). Phase III is the INT phase, in which both symmetry breakings occur: $\eta \neq 0$ (3*c*) and $\xi \neq 0$ (5*b*). We could not detect phase II, in which only $\xi \neq 0$. The phase diagram shown in Figure 10 corresponds to the case of a strong negative coupling between the two order parameters ($\gamma > 0$), for which a thermodynamic path is theoretically possible, such as α–α' from phase 0 to phase III through a first-order transition. Such a phase transition is theoretically limited to a first-order transition line. It is clear from Figure 7 that this phase transition from phase 0 (HS) to III (INT) has a first-order signature, as the volume (intensity of Bragg reflections) varies discontinuously.

In the phase diagram (Figure 10) for two coupled OPs (η, ξ), some thermodynamic path allows the sequence of phases 0–III–I,[28] but it is not observed here at thermal equilibrium. Phase I, which results from photoinduced spin-state switching at low temperature, can only be reached through light-control of the internal variable n_{HS}. The metastable HS state at low temperature (phase I characterized by $\eta \neq 0$ and $\xi = 0$) may only be reached in the photoinduced HS state when the value of n_{HS} reaches 1. As phase I cannot be reached through the thermodynamic equilibrium path, but only by photo-excitation at low temperature, a complete description of such out-of-equilibrium dynamics would require, for example, the use of a dynamic potential approach,[29] and the introduction of a symmetry-breaking OP. This represents a theoretical challenge and goes far beyond the scope of the present paper.

Because the LS state is characterized by a quadruplicate *a* parameter, describing the thermodynamic path from phase III to the LT phase would require the use of a third symmetry-breaking OP (ε). In such a case, one should supplement Equation (1) with even terms in ε. Therefore, the phase diagram sketched in Figure 10 as a two-dimensional plot for two symmetry-breaking OPs would become a three-dimensional plot for three OPs, with a c_1 axis perpendicular to the figure. The thermodynamic path between high and low temperature would then reach phase 0 (HS) and III (INT), and would cross another first-order transition toward phase IV (LS, $\eta = 0$, $\xi = 0$, $\varepsilon \neq 0$) at lower temperature.

Conclusion

The present results illustrate how electronic instabilities (HS vs. LS) can compete and couple with structural instabilities (ordering of distorted molecules) to generate new phases. The relative population of HS/LS states depends on temperature, but can also be controlled by light, yielding a metastable HS state at low temperature, at which the LS state is the true ground state. In addition, as observed in many systems in nature, structural ordering of distorted molecules can take place between disordered (HT) and ordered (LT) phases, resulting in symmetry breaking. In the present case, light allows to overcome a thermodynamic path for reaching new states, and to decouple the two phenomena by generating the metastable HS state at low temperature, thus allowing observation of the broken-symmetry HS phase.

Another illustration of such competing phenomena is the appearance of the intermediate phase resulting from spin-state ordering. The supercell structure presented here is unusual since it is associated with a unit-cell multiplication from (*a*, *b*, *c*) to (*a*, 5*b*, 3*c*). The related long-range order that arises involves several structural degrees of freedom, as well as a spatial distribution of HS and LS molecules. In the present case, the long-range ordering of the INT phase is based on the competition between two symmetry-breaking order parameters. As a result, an unprecedented lozenge pattern of HS molecules confines molecules in the LS state. To date, there have been scarce attempts to describe such phenomena[30] by considering competition between different sub-lattices and different intra- and inter-sub-lattice interactions. The universal Landau theory of phase transitions has been used[31] to demonstrate how the HS fraction n_{HS} (a totally symmetrical OP) can couple to one symmetry-breaking OP η to generate HS-LS ordering. In the present case, a more complex description would be required since n_{HS} has

to couple with both η and ξ. If the concept of sub-lattice has been easy to define for the examples reported to date,[12b,16,20,25] it is not so easy in the present case: increasing the number of order parameters increases the difficulty in describing a phase diagram. This is another illustration that in such multistable systems different false ground states compete.

Finally, comparison of the isostructural compounds **1** and **2** shows that they differ only in their intermediate phase. It was underlined for **2**,[20] but it is also true for **1**, that N–H···F bonds involving both imidazole and amine moieties of the ligand play an important role in driving rotations/displacements of the ions as symmetry is broken. In the case of **1**, important frustrations and competitions exist between spin conversion and ion rotation, mostly related to space limitation: the AsF_6 anion (**1**) is larger than PF_6 (**2**).[20] This interaction competes with HS-LS ordering, revealing another type of order parameter in the INT phase of **1**.

Experimental Section

Synthesis: The $H_2L^{2\text{-Me}}$ ligand was prepared as previously described,[21] by Schiff-base condensation of *N*,*N*′-bis(3-aminopropyl)ethylenediamine (174 mg, 1 mmol) with 2-methyl-4-formylimidazole (220 mg, 2 mmol) in ethanol (10 mL). The freshly prepared pale-yellow solution of Schiff-base ligand was deoxygenated prior to complexation reactions in a glove box. Orange crystals of **1** were obtained as follows.[20] A solution of $Fe^{II}Cl_2{\cdot}4H_2O$ (198 mg, 1 mmol) in ethanol (5 mL) was added to a solution of $H_2L^{2\text{-Me}}$ (1 mmol) in ethanol (10 mL) with stirring and heating (ca. 45–50 °C). After 30 min, a solution of $NaAsF_6$ (423 mg, 2 mmol) in ethanol (10 mL) was added dropwise to the reaction mixture. The resulting mixture was stirred and heated for a further 1 h and then filtered. The filtrate was allowed to stand for several days, and the orange crystals that formed were collected by filtration. X-ray quality dark-orange crystals of **1** were obtained in 51 % yield (390 mg). Elemental analysis calcd (%) for **1**, $FeC_{18}H_{30}N_8As_2F_{12}$, 792.2 g mol^{-1}: C 27.29, H 3.82, N 14.15; found: C 27.14, H 3.45, N 14.25; IR (KBr): $\tilde{\nu}$ = 1633 (C=N), 705 cm^{-1} (AsF_6).

Physical measurements: C, H, and N elemental analyses were carried out on a Perkin–Elmer 2400 series II analyzer. Infrared spectra were recorded at room temperature using a Perkin–Elmer 9800 FTIR spectrometer with samples in KBr disks (% transmittance) or directly as microcrystalline powders (attenuated total reflectance). Magnetic susceptibilities were measured in the 2–300 K temperature range, at a sweep rate of 2 K min^{-1}, under an applied magnetic field of 1 T, using an MPMS5 SQUID susceptometer (Quantum Design). The apparatus was calibrated with palladium metal. Corrections for diamagnetism were applied by using Pascal's constants. The photomagnetic study of **1** was carried out using a 532 nm continuous-wave laser coupled through an optical fiber into the cavity of the susceptometer. The sample was prepared as a thin layer (mass ≈0.93 mg) to optimize the penetration of irradiation light. The sample weight was then obtained by comparing its thermal SC with that of a heavier and accurately weighed sample.[22] The sample was first slowly cooled to 10 K, to avoid any thermal quench and attainment of the fully LS state. Irradiation up to photosaturation was carried out with a 10 mW cm^{-2} power intensity. Then, in the absence of irradiation, the temperature was increased at 1 K min^{-1} up to 50 K, whereupon **1** reached its fully LS state. Mössbauer spectra were recorded on a constant acceleration conventional spectrometer with a 50 mCi source of ^{57}Co (Rh matrix). A least-squares computer program[24] was used to fit the Mössbauer parameters and to determine their standard deviation of statistical origin (given in parentheses). Isomer shift values are quoted relative to iron foil at 293 K.

X-ray diffraction analysis: Experiments were performed on single crystals with an Xcalibur 3 four-circle diffractometer (Oxford Diffraction). The crystals were mounted in an Oxford Cryosystems nitrogen-flow cryostat for measurements down to 80 K (temperature stability of 0.1 K) and an Oxford Diffraction Helijet helium-flow cryostat was used to determine the structure at 15 K (temperature stability of 1 K). A 532 nm laser was used to generate the photoinduced HS state at 15 K. The unit-cell parameters and data reduction were obtained with the CrysAlis software from Oxford Diffraction.[32] The structures were solved by direct methods with SIR-97[33] and refined against F^2 by full-matrix least-squares techniques using SHELXL-97[34] with anisotropic displacement parameters for all non-hydrogen atoms. CCDC-714013 (HS-250 K), 760827 (INT-100 K), 714011 (LS-15 K), and 760828 (PIHS-15 K-532 nm) contain the supplementary crystallographic data for this paper. These data can be obtained free of charge from The Cambridge Crystallographic Data Centre via www.ccdc.cam.ac.uk/data_request/cif.

Acknowledgements

This work was supported by Grants in Aid for Scientific Research (no.: 16205010) from the Ministry of Education, Science, Sports, and Culture, Japan, Grants in Aid for Creative Scientific Research Program (no.: 18GS0208) from the Ministry of Education, Science, Sports, and Culture, Japan, the Institut Universitaire de France, and a Grant "CREATE Ultimate" No. 4146 from Région Bretagne, France. N.B. is grateful to the JSPS for providing a Foreign Postdoctoral Fellowship.

[1] a) M. D. Hollingsworth, K. D. M. Harris, *Comprehensive Supramolecular Chemistry*, Vol. 6 (Eds.: D. D. MacNicol, F. Toda, R. Bishop), Pergamon, Oxford, **1996**, pp. 177–237; b) K. D. M. Harris, *Supramol. Chem.* **2007**, *19*, 47–53; c) M. Marschall, J. Reichert, A. Weber-Bargioni, K. Seufert, W. Auwärter, S. Klyatskaya, G. Zoppellaro, M. Ruben, J. V. Barth, *Nat. Chem.* **2010**, *2*, 131–137; d) B. Toudic, P. Garcia, C. Odin, P. Rabiller, C. Ecolivet, E. Collet, P. Bourges, G. J. McIntyre, M. D. Hollingsworth, T. Breczewski, *Science* **2008**, *316*, 69–71.

[2] a) M. Verdaguer (Ed.), "New Trends in Molecular Magnetism", *C. R. Chimie* **2008**, *11*, 1083–1300; b) A. Dei, *Angew. Chem.* **2005**, *117*, 1184–1187; *Angew. Chem. Int. Ed.* **2005**, *44*, 1160–1163; c) O. Sato, *Acc. Chem. Res.* **2003**, *36*, 692–700.

[3] a) P. Gütlich, H. A. Goodwin, *Top. Curr. Chem.* **2004**, *233*, 1–47; b) J.-F. Létard, P. Guionneau, L. Goux-Capes, *Top. Curr. Chem.* **2004**, *235*, 221–249.

[4] M. B. Duriska, S. M. Neville, B. Moubaraki, J. D. Cashion, G. J. Halder, K. W. Chapman, C. Baldé, J. F. Létard, K. S. Murray, C. J. Kepert, S. R. Batten, *Angew. Chem.* **2009**, *121*, 2587–2590; *Angew. Chem. Int. Ed.* **2009**, *48*, 2549–2552.

[5] G. Molnár, S. Cobo, J. A. Real, F. Carcenac, E. Daran, C. Vieu, A. Bousseksou, *Adv. Mater.* **2007**, *19*, 2163–2167.

[6] I. Boldog, A. B. Gaspar, V. Martínez, P. Pardo-Ibañez, V. Ksenofontov, A. Bhattacharjee, P. Gütlich, J. A. Real, *Angew. Chem.* **2008**, *120*, 6533–6537; *Angew. Chem. Int. Ed.* **2008**, *47*, 6433–6437.

[7] a) E. Coronado, J. R. Galán-Mascarós, M. Monrabal-Capilla, J. García-Martinez, P. Pardo-Ibáñez, *Adv. Mater.* **2007**, *19*, 1359–1361; b) T. Forestier, S. Mornet, N. Daro, T. Nishihara, S.-I. Mouri, K. Tanaka, O. Fouché, E. Freysz, J.-F. Létard, *Chem. Commun.* **2009**, 4327–4329.

[8] a) J. Larionova, L. Salmon, Y. Guari, A. Tokarev, K. Molvinger, G. Molnár, A. Bousseksou, *Angew. Chem.* **2008**, *120*, 8360–8364; *Angew. Chem. Int. Ed.* **2008**, *47*, 8236–8240; b) F. Volatron, L. Catala, E. Rivière, A. Gloter, O. Stéphan, T. Mallah, *Inorg. Chem.* **2008**, *47*, 6584–6586; c) S. M. Neville, C. Etrillard, S. Asthana, J.-F. Létard, *Eur. J. Inorg. Chem.* **2010**, 282–288.

[9] a) H. Spiering, *Top. Curr. Chem.* **2004**, *235*, 171–195, and references therein; b) N. Klinduhov, D. Chernyshov, K. Boukheddaden, *Phys. Rev. B* **2010**, *81*, 094408.
[10] a) G. Lemercier, M. Verelst, A. Bousseksou, F. Varret, J.-P. Tuchagues, in *Magnetism: A Supramolecular Function*, Vol. 484 (Ed.: O. Kahn), NATO ASI Series C, Kluwer Academic Publishers, Dordrecht, **1996**, 335–356; b) S. Hayami, Z. Gu, M. Shiro, Y. Einaga, A. Fujishima, O. Sato, *J. Am. Chem. Soc.* **2000**, *122*, 7126–7127; c) S. Hayami, Z. Gu, H. Yoshiki, A. Fujishima, O. Sato, *J. Am. Chem. Soc.* **2001**, *123*, 11644–11650; d) Y. Sunatsuki, Y. Ikuta, N. Matsumoto, H. Ohta, M. Kojima, S. Iijima, S. Hayami, Y. Maeda, S. Kaizaki, F. Dahan, J.-P. Tuchagues, *Angew. Chem.* **2003**, *115*, 1652–1656; *Angew. Chem. Int. Ed.* **2003**, *42*, 1614–1618; e) G. Lemercier, N. Bréfuel, S. Shova, J. Wolny, F. Dahan, M. Verelst, H. Paulsen, A. X. Trautwein, J.-P. Tuchagues, *Chem. Eur. J.* **2006**, *12*, 7421–7432; f) N. Bréfuel, S. Shova, J. Lipkowski, J.-P. Tuchagues, *Chem. Mater.* **2006**, *18*, 5467–5479; g) N. Bréfuel, S. Shova, J.-P. Tuchagues, *Eur. J. Inorg. Chem.* **2007**, 4326–4334.
[11] a) J. Kröber, E. Codjovi, O. Kahn, F. Grolière, C. Jay, *J. Am. Chem. Soc.* **1993**, *115*, 9810–9811; b) J. G. Haasnoot, in *Magnetism: A Supramolecular Function*, Vol. 484 (Ed.: O. Kahn), NATO ASI Series C, Kluwer Academic Publishers, Dordrecht, **1996**, 299–321; c) J. A. Real, A. B. Gaspar, V. Niel, M. C. Muñoz, *Coord. Chem. Rev.* **2003**, *236*, 121–141; d) J.-A. Real, A. B. Gaspar, M.-C. Muñoz, P. Gütlich, V. Ksenofontov, H. Spiering, *Top. Curr. Chem.* **2004**, *233*, 167–193, and references therein.
[12] a) O. Kahn, C. Jay-Martinez, *Science* **1998**, *279*, 44–48; b) D. Boinnard, A. Bousseksou, A. Dworkin, J.-M. Savariault, F. Varret, J.-P. Tuchagues, *Inorg. Chem.* **1994**, *33*, 271–281; c) L. G. Lavrenova, N. G. Yudina, V. N. Ikorskii, V. A. Varnek, I. M. Oglezneva, S. V. Larionov, *Polyhedron* **1995**, *14*, 1333–1337.
[13] S. Hayami, K. Danjobara, K. Inoue, Y. Ogawa, N. Matsumoto, Y. Maeda, *Adv. Mater.* **2004**, *16*, 869–872.
[14] K. Nasu (Ed.), *Relaxation of Excited States and Photoinduced Structural Phase Transitions*, Springer, Berlin, Heidelberg, **1997**.
[15] a) P. Guionneau, M. Marchivie, G. Bravic, J. F. Létard, D. Chasseau, *Top. Curr. Chem.* **2004**, *234*, 97–128; b) J. Kusz, P. Gütlich, H. Spiering, *Top. Curr. Chem.* **2004**, *234*, 129–153.
[16] S. Neville, B. Leita, G. Halder, C. Kepert, B. Moubaraki, J.-F. Létard, K. S. Murray, *Chem. Eur. J.* **2008**, *14*, 10123–10133.
[17] D. Chernyshov, M. Hostettler, K. W. Törnroos, H.-B. Bürgi, *Angew. Chem.* **2003**, *115*, 3955–3960; *Angew. Chem. Int. Ed.* **2003**, *42*, 3825–3830.
[18] a) M. Yamada, M. Ooidemizu, Y. Ikuta, S. Osa, N. Matsumoto, S. Iijima, M. Kojima, F. Dahan, J.-P. Tuchagues, *Inorg. Chem.* **2003**, *42*, 8406–8416; b) M. Yamada, H. Hagiwara, H. Torigoe, N. Matsumoto, M. Kojima, F. Dahan, J.-P. Tuchagues, N. Re, S. Iijima, *Chem. Eur. J.* **2006**, *12*, 4536–4549.
[19] S. Bonnet, M. A. Siegler, J. S. Costa, G. Molnár, A. Bousseksou, A. L. Spek, P. Gamez, J. Reedijk, *Chem. Commun.* **2008**, 5619–5621.
[20] N. Bréfuel, H. Watanabe, L. Toupet, J. Come, N. Matsumoto, E. Collet, K. Tanaka, J.-P. Tuchagues, *Angew. Chem.* **2009**, *121*, 9468–9471; *Angew. Chem. Int. Ed.* **2009**, *48*, 9304–9307.
[21] N. Bréfuel, S. Imatomi, H. Torigoe, H. Hagiwara, S. Shova, J.-F. Meunier, S. Bonhommeau, J.-P. Tuchagues, N. Matsumoto, *Inorg. Chem.* **2006**, *45*, 8126–8136.
[22] J. F. Létard, *J. Mater. Chem.* **2006**, *16*, 2550–2559.
[23] S. Decurtins, P. Gütlich, C. P. Kohler, H. Spiering, A. Hauser, *Chem. Phys. Lett.* **1984**, *105*, 1–4.
[24] K. Lagarrec, *Recoil*, *Mössbauer Analysis Software for Windows*, available via the internet at http://www.physics.uottawa.ca/_recoil.
[25] a) E. Collet, M. Buron-Le Cointe, H. Cailleau, *J. Phys. Soc. Jpn.* **2006**, *75*, 011002; b) M. Lorenc, J. Hebert, N. Moisan, E. Trzop, M. Servol, M. Buron-Le Cointe, H. Cailleau, M. L. Boillot, E. Pontecorvo, M. Wulff, S. Koshihara, E. Collet, *Phys. Rev. Lett.* **2009**, *103*, 028301; c) T. Elsaesser, M. Woermer, *Acta Crystallogr. Sect. A* **2010**, *66*, 168–178; d) P. Coppens, J. Benedict, M. Messerschmidt, I. Novozhilova, T. Graber, Y. S. Chen, I. Vorontov, S. Scheins, S. L. Zheng, *Acta Crystallogr. Sect. A* **2010**, *66*, 179–188; e) E. Collet, M. Buron-Le Cointe, M. Lorenc, H. Cailleau, *Z. Kristallogr.* **2008**, *223*, 272–282.
[26] a) C.-F. Sheu, S.-M. Chen, S.-C. Wang, G.-H. Lee, Y.-H. Liu, Y. Wang, *Chem. Commun.* **2009**, 7512–7514; b) C. H. Shih, C. F. Cheu, K. Kato, K. Sugimoto, J. Kim, Y. Wang, M. Takata, *Dalton Trans.* **2010**, *39*, 9794–9800.
[27] A. J. Simaan, M.-L. Boillot, R. Carrasco, J. Cano, J.-J. Girerd, T. A. Mattioli, J. Ensling, H. Spiering, P. Gütlich, *Chem. Eur. J.* **2005**, *11*, 1779–1793.
[28] Y. M. Gufan, E. S. Larin, *Sov. Phys. Solid State* **1980**, *22*, 270–275.
[29] K. Boukheddaden, I. Sheto, B. Hôo, F. Varret, *Phys. Rev. B* **2000**, *62*, 14806.
[30] M. Nishino, K. Boukheddaden, S. Miyashita, *Phys. Rev. B* **2003**, *68*, 224402.
[31] D. Chernyshov, H.-B. Bürgi, M. Hostettler, K. Törnoos, *Phys. Rev. B* **2004**, *70*, 094116.
[32] *CrysAlis RED*, Oxford Diffraction Ltd., Version 1.171.32.5, **2007**.
[33] A. Altomare, M. C. Burla, M. Camalli, G. Cascareno, G. Giacovazzo, A. Guagliardi, A. G. G. Moliterni, G. Polidori, R. Spagna, *J. Appl. Crystallogr.* **1999**, *32*, 115–119.
[34] G. M. Sheldrick, *SHELXL-97*, Program for the refinement of crystal structures from diffraction data, University of Göttingen, Germany, **1997**.

Received: May 10, 2010
Published online: November 12, 2010

